SENRA Academic Publishers, Burnaby, British Columbia
Vol. 3, No. 1, pp. 731-739, 2009
ISSN: 1715-9997

Canadian Journal of pure&applied sciences

EFFECTS OF ENGINE SPEED ON INJECTION TIMING AND ENGINE PERFORMANCE FOR 4-CYLINDER DIRECT INJECTION HYDROGEN FUELED ENGINE

M M Rahman, Mohammed K Mohammed and Rosli Abu Bakar
Faculty of Mechanical Engineering, Universiti Malaysia Pahang
Tun Abdul Razak Highway, 26300 Gambang, Kuantan, Pahang, Malaysia

ABSTRACT

In this study, the effects of engine speed on the injection timing and engine performance of 4-cylinder direct injection (DI) hydrogen fueled engine were investigated. The 4-cylinder direct injection hydrogen engine model was developed utilizing the GT-Power commercial software. This model was employed one dimensional gas dynamics to represent the flow and heat transfer in the components of engine model. Sequential pulse injectors was adopted to the inject hydrogen gas fuel within the compression stroke. Injection timing was varied from 110^0 before top dead center (BTDC) until 0^0 top dead center (TDC) timing. Engine speed was varied from 2000 rpm to 6000 rpm. The validation was performed with the existing previous experimental results. The negative effects of the interaction between ignition timing and injection duration was highlighted and clarified. The acquired results show that the engine speeds are strongly influence on the injection timing and engine performance. It can be seen that the indicated efficiency increases with decreases of engine speed; power increases with the decreases of engine speed; indicated specific fuel consumption (ISFC) increases with increases of engine speed. The injection timing of 60^0 BTDC was the overall optimum injection timing with a compromise.

Keywords: Direct injection engine, injection timing, engine performance, engine speed, hydrogen fueled.

INTRODUCTION

With increasing concern about the energy shortage and environmental protection, research on improving engine fuel economy, hydrogen fueled engine is being developed into a hydrogen fueled engine with manifold injection, direct injection or duel injection according to the fuel supply method (Lee *et al.*, 2002; William *et al.*, 2002; Eichlseder *et al*., 2003; Kim *et al.*, 2005). Of course, the hydrogen fueled engine with direct injection can fundamentally keep backfires from occurring so it can be utilized as a high powered hydrogen power system if the reliability of high pressure direct injection valve is secured (MacCarley and Van Vorst, 1980; Lee *et al*., 2001). Hydrogen gas is characterized by a rapid combustion speed, wide combustible limit and low minimum ignition energy. Such characteristics play a role to decrease engine cycle variation for the safety of combustion. However, it is frequently observed that the values of cycle variation for hydrogen fueled engines with direct injection are higher than those of hydrogen fueled engines with manifold injection or those of gasoline engines, due to a decrease in the mixing period by direct injection in the process of compressing hydrogen gas (Nakagawa *et al*., 1982; Kim *et al*., 1995; Varde and Frame, 1985). In today's modern world, where new technologies are introduced every day, transportation's energy use is increasing rapidly. Fossil fuel particularly petroleum fuel is the major contributor to energy production and the primary fuel for transportation. Rapidly depleting reserves of petroleum and decreasing air quality raise questions about the future. As world awareness about environment protection increases so does the search for alternative to petroleum fuels. Hydrogen can be used as a clean alternative to petroleum fuels and its use as a vehicle fuel is promising in the effects to establish environmentally friendly mobility systems. So far, the extensive studies were investigated hydrogen fueled internal combustion engines (H_2ICE) with external mixture formation fuel delivery system (Stockhausen *et al*., 2002; Kahraman *et al*., 2007). However, the operation of these engines subjected to abnormal combustion, such as pre-ignition, backfire and knocking. Moreover, the power outputs of these hydrogen engines are about 30% less than those of gasoline engines (Tang *et al*., 2002). Therefore the premixed-charge spark ignition engines fueled with hydrogen can be used for significantly limited operation range (Tsujimura *et al*., 2003). It is a common conclusion achieved by many researchers that abnormal combustion can be controlled by direct injection (DI) of hydrogen inside the cylinder (Tsujimura *et al*., 2003; Rottengruber *et al*., 2004; Mohammadi *et al*., 2007).

Direct injection H_2ICE requires optimized operation strategies that enable the availability of high power output as well as the abolition of critical exhaust gas emission in

*Corresponding author email: mustafizur@ump.edu.my

combination with high efficiencies. Several parameters need to be optimized. Optimization of spark timing, valve timing, combustion chamber geometry, injection parameters such as injection timing, injection duration, injection pressure and nozzle hole numbers/arrangement, swirls intensity, etc. are indeed important to achieve an engine performance level competitive to that in the modern direct-injection diesel engines (Mohammadi *et al*., 2007).

Injection timing plays a critical role in the phasing of the combustion, and hence the emissions and torque production. Therefore, extensive number of studies indicated the significance of optimization for ignition timing (Sierens *et al*., 2005; Kim *et al*., 2006; White *et al*., 2006; Mohammadi *et al*., 2007; White *et al*., 2006) suggested that late injection can minimize the residence time that a combustible mixture is exposed to in-cylinder hot spots and allow for improved mixing of the intake air with the residual gases. This selection can control pre-ignition problem. The main challenge for selecting proper ignition timing that is in-cylinder injection requires hydrogen–air mixing in a very short time. For early injection (i.e., coincident with inlet valve closure (IVC)), maximum available mixing times range from approximately 20 ms to 4 ms across the speed range 1000 rpm to 5000 rpm. In practice, to avoid pre-ignition, start of injection (SOI) is retarded with respect to IVC and mixing times are further reduced. Regarding the behavior of the performance characteristic with ignition timing, there are several contradictories in the literature. Eichlseder *et al*. (2003) found that at low loads (or low equivalence ratio (ϕ)), indicated efficiency (IE) increases with retard of SOI. The increase was shown to be due to the decrease in the compression work caused by differences in mixture gas properties and charge mass with retarded SOI. Eichlseder *et al*. (2003) also found their study at high loads, IE first increases and then decreases with retard of SOI. The reversing trend is assumed to be a consequence of an unfavorable mixture formation. However, Kim *et al*. (2006) reported the results contradictory to Eichlseder *et al*. (2003) results, where they find that, for both low and high loads, indicated efficiency decreases monotonically with retard of SOI. These contradictory findings may be a result of differences in mixture formation (White *et al*., 2006). Much effort has been devoted to optimize the injection timing which is ranging from IVC until the top dead center (i.e. within the compression stroke). However, Mohammadi *et al*. (2007) optimized the injection timing for three ranges:

- during the intake stroke, where they prevented backfire. However, thermal efficiency and output power are limited by knock due to reduction in volumetric efficiency;
- at compression stroke, where they prevented knock and gives an increase in thermal efficiency and maximum output power; and

at later stage of compression stroke, where they achieved thermal efficiency higher than 38.9% and brake mean effective pressure 0.95MPa.

This study attempts to optimize injection timing that gives the best performance of a 4-cylinders direct injection. The 4-cylinder direct injection hydrogen fueled engine model is developed for this purpose. The effects of engine speed on the injection timing and engine performance such as indicated efficiency indicated specific fuel consumption, power and torque for direct injection hydrogen fueled engine.

MODEL DESCRIPTION

The engine model for an in-line 4-cylinder direct injection engine was developed for this study. Engine specifications for the base engine are tabulated in Table 1. The specific values of input parameters including the AFR, engine speed, and injection timing were defined in the model. The boundary condition of the intake air was defined first in the entrance of the engine. The air enters through a bell-mouth orifice to the pipe. The discharge coefficients of the bell-mouth orifice were set to 1 to ensure the smooth transition as in the real engine. The pipe of bell-mouth orifice with 0.07 m of diameter and 0.1 m of length are used in this model. The pipe connects in the intake to the air cleaner with 0.16 m of diameter and 0.25 m of length was modeled. The air cleaner pipe identical to the bell-mouth orifice connects to the manifold. A log style manifold was developed from a series of pipes and flow-splits. The intake system of the present study model is shown in Fig. 1. The total volume for each flow-split was 256 cm^3. The flow-splits compose from an intake and two discharges. The intake draws air from the preceding flow-split. One discharge supplies air to adjacent intake runner and the other supplies air to the next flow-split. The last discharge pipe was closed with a cup to prevent any flow through it because there is no more flow-split. The flow-splits are connected with each other via pipes with 0.09 m diameter and 0.92 m length. The junctions between the flow-splits and the intake runners were modeled with bell-mouth orifices. The discharge coefficients were also set to 1 to assure smooth transition, because in most manifolds the transition from the manifold to the runners is very smooth. The intake runners for the four cylinders were modeled as four identical pipes with .04 m diameter and 0.1 m length. Finally the intake runners were linked to the intake ports which were modeled as pipes with 0.04 m diameter and 0.08 lengths. The air mass flow rate in the intake port was used for hydrogen flow rate based on the imposed AFR.

Table 1. Engine specification.

Engine Parameter	Value	Unit
Bore	100	mm
Stroke	100	mm
Connecting rod length	220	mm
Piston pin offset	1.00	mm
Total displacement	3142	(cm^3)
Compression ratio	9.5	
Inlet valve close, IVC	-96	^{0}CA
Exhaust valve open, EVO	125	^{0}CA
Inlet valve open, IVO	351	^{0}CA
Exhaust valve close, EVC	398	^{0}CA

The second major part of the engine model is the powertrain model which is shown in figure 2. In the powertrain, the induced air passes through the intake cam-driven type valves with 45.5 mm of diameter to the cylinders. The valve lash (mechanical clearance between the cam lobe and the valve stem) was set to 0.1 mm. The overall temperature of the head, piston and cylinder for the engine parts are listed in table 2. The temperature of the piston is higher than the cylinder head and cylinder block wall temperature because this part is not directly cooled by the cooling liquid or oil. The burning rate (X_b) of combustion process was modeled using Wiebe function, which can be expressed as Eq. (1):

Table 2. Temperature of the mail engine parts.

Components	Temperature (K)
Cylinder head	550
Cylinder block wall	450
Piston	590

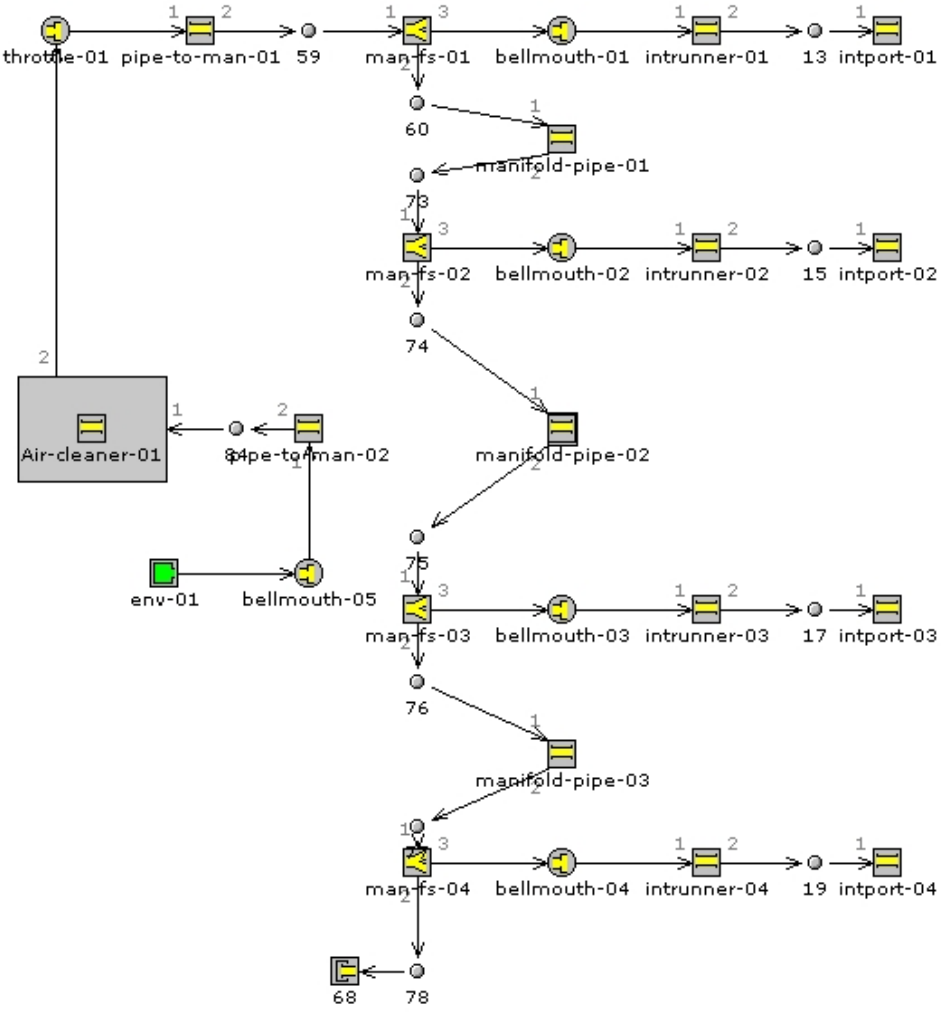

Fig. 1. Intake system model.

$$X_b = 1 - \exp\left[-a\left(\frac{\theta - \theta_i}{\Delta\theta}\right)^{n+1}\right] \quad (1)$$

where θ is the crank angle, θ_i is the start of combustion, $\Delta\theta$ is the combustion period and *a* and *n* are adjustable constants.

Furthermore, the heat transfer in-side the cylinder was modeled using a formula which is closely emulates the classical Woschni correlation. Based on this correlation, the heat transfer coefficient h_c can be expressed as Eq. (2):

$$h_c = 3.26B^{-0.2}p^{0.8}T^{-0.55}w^{0.8} \quad (2)$$

where *B* is the bore in meters, *p* is the pressure in kPa, *T* is temperature in K and *w* is the average cylinder gas velocity in m/s.

The hydrogen gas fuel was injected directly in-side the cylinders using the four sequential pulse fuel injectors. The AFR was imposed for the injectors. Then, the injected fuel rate was estimated using the Eq. (3):

$$\dot{m}_{\text{delivery}} = \eta_v \rho_{\text{ref}} N V_d (FAR) \frac{3}{2(PW)} \quad (3)$$

where $\dot{m}_{\text{delivery}}$ is the injector delivery rate (g/s), ρ_{ref} the reference density (kg/m^3), *N* is the engine speed (rpm), V_d is the volume displacement (cm^3), *FAR* is the fuel air ratio and *PW* is the injection duration (^{0}CA).

The four cylinders were then connected together through the engine part which translates the force acting on each piston into the crankshaft (brake) power. Furthermore, engine friction model was imposed to model friction in the engine. The friction mean effective pressure *(FMEP)* was modeled based on Eq. (4):

$$FMEP = 0.4 + (0.005 \times P_{\max}) + (0.09 \times Speed_{mp}) + (0.0009 \times Speed^2_{mp}) \quad (4)$$

where $Speed_{mp}$ represents the mean piston speed and P_{max} is the peak cylinder pressure.

The last major part in the present model is the exhaust system which is shown in figure 3. The exhaust runners were modeled as rounded pipes with 0.03 m inlet diameter, and 80^0 bending angle for runners 1 and 4; and 40^0 bending angle of runners 2 and 3. Runners 1 and 4, and runners 2 and 3 are connected before enter in a flow-split with 169.646 cm^3 volume. Conservation of momentum is solved in 3-dimentional flow-splits even though the flow in GT-Power is otherwise based on a one-dimensional version of the Navier-Stokes equation. Finally a pipe with 0.06 m diameter and 0.15 m length connects the last flow-split to the environment. Exhaust system walls temperature was calculated using a model embodied in each pipe and flow-split. Table 3 are listed the parameters used in the exhaust environment of the model. Figure 4 shows the entire model of 4-cylinder direct injection engine.

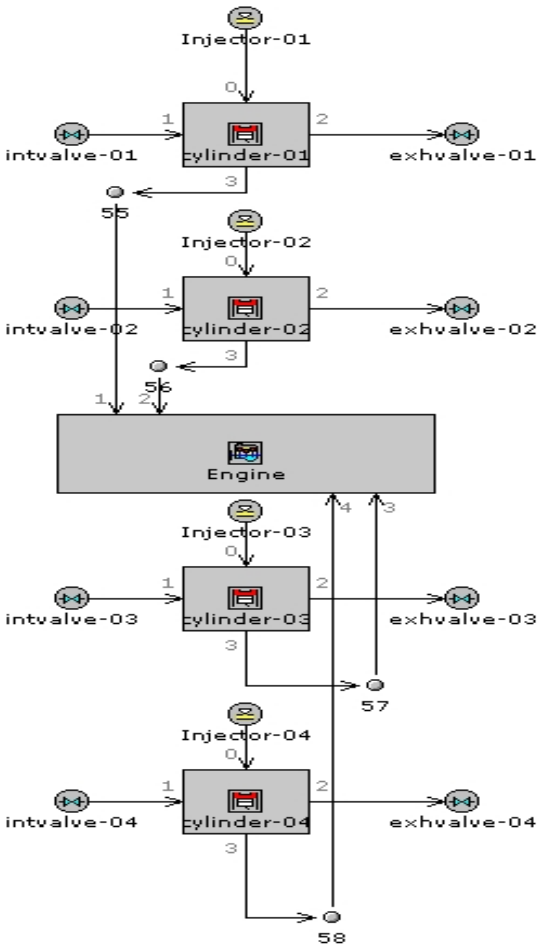

Fig. 2. Powertrain model.

Table 3. Parameters used in the exhaust environment.

Parameters	Value	Unit
External environment temperature	320	K
Heat transfer coefficient	15	W/m^{2}K
Radiative temperature	320	K
Wall layer material	Steel	
Layer thickness	3	Mm
Emissivity	0.8	

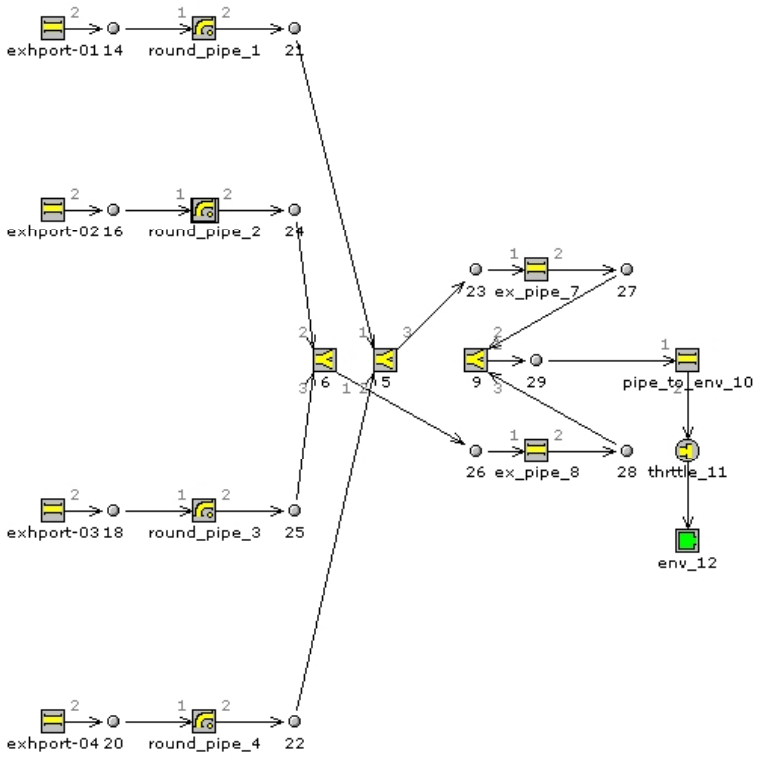

Fig. 3. Exhaust system model.

RESULTS AND DISCUSSION

The results in the following section show the engine performance behavior with injection timing for each condition under investigation. In order to check the validity and accuracy of the present model, comparison with published experimental results in the literature. The effect of AFR with injection timing on the engine performance parameters including efficiency, brake specific fuel consumption, power, and torque were discussed. The effects of engine speed with injection timing on the engine performances are also investigated.

Model Validation

The experimental results obtained from Mohammadi *et al*. (2007) were used for the purpose of validation in this study. Engine specifications of Mohammadi *et al*. (2007) and present single cylinder direct injection engine model are listed in Table 4. For the purpose of validation, single cylinder direct injection engine model converted to 4-cylinder direct injection model. Figure 5 shows the single cylinder direct injection engine model. Engine speed and AFR were fixed at 1200 rpm and 57.216 ($\theta = 0.6$) respectively in this comparison. Injection timing was varied from 130 ^{0}CA BTDC until 70 ^{0}CA BTDC to be coincident with Mohammadi *et al*. (2007). The correlation of brake thermal efficiency of the baseline model and experimental results obtained from Mohammadi *et al*. (2007) is shown in Fig. 6. It can be seen that the brake thermal efficiency are good match with the experimental results. Only small deviation was obtained due to the difference between the engine operation conditions that are not mentioned in Mohammadi *et al*. (2007). However, considerable coincident between the single cylinder model and experimental results can be recognized in spite of the mentioned model differences.

Table 4. Specifications of the engines models.

Engine Parameter	Mohammadi *et al*. (2007)	Present Model	Unit
Bore	102	102	mm
Stroke	105	105	mm
Connecting rod length	NA*	220	mm
Piston pin offset	NA	1.00	mm
Total displacement	857	858	(cm^3)
Compression ratio	11.5	11.5	
Inlet valve close, IVC	580	624^0	ATDC
Exhaust valve open, EVO	130	125^0	ATDC
Inlet valve open, IVO	360	351^0	ATDC
Exhaust valve close, EVC	380	398^0	ATDC

* NA = not available

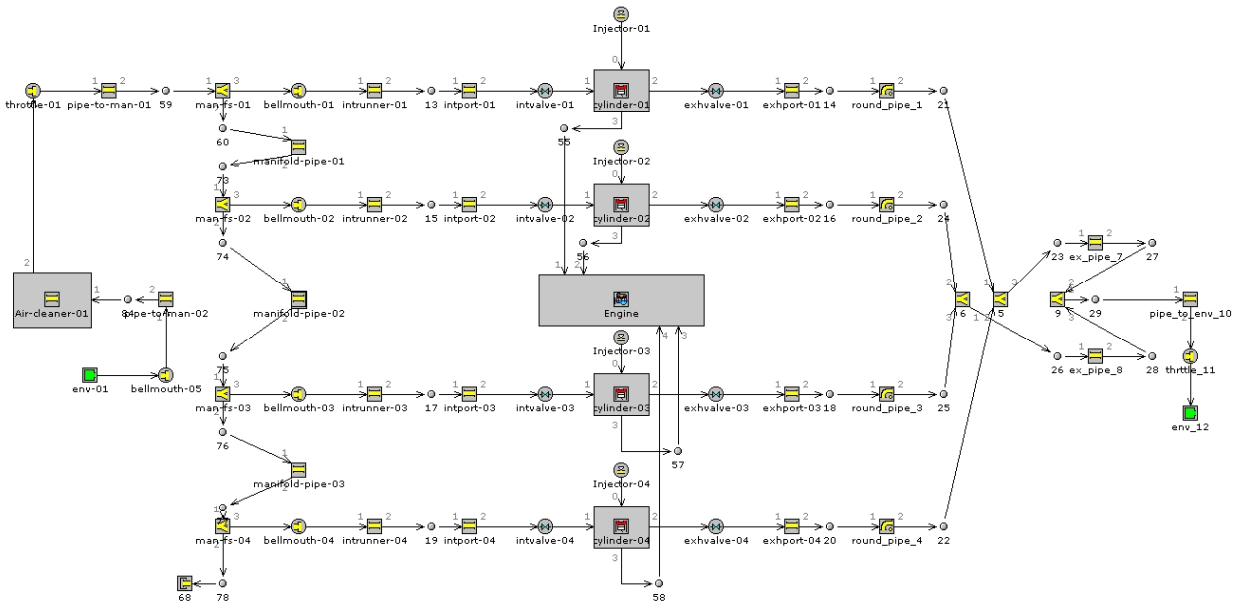

Fig. 4. In-line 4-cylinder direct injection hydrogen fueled engine model.

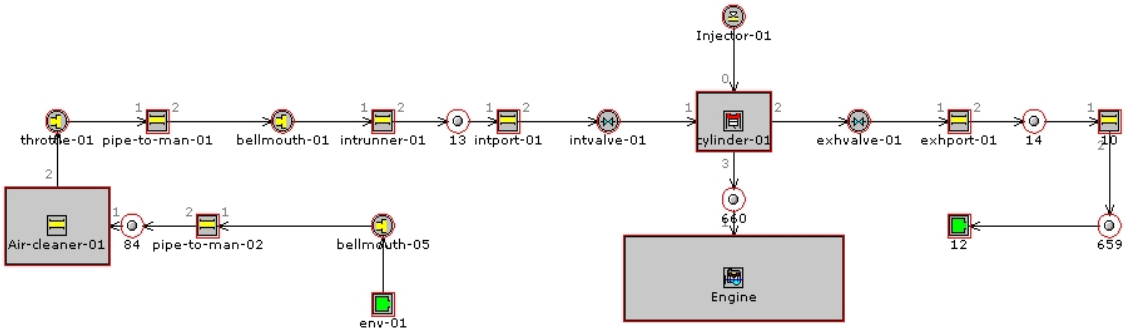

Fig. 5. Single cylinder direct injection model.

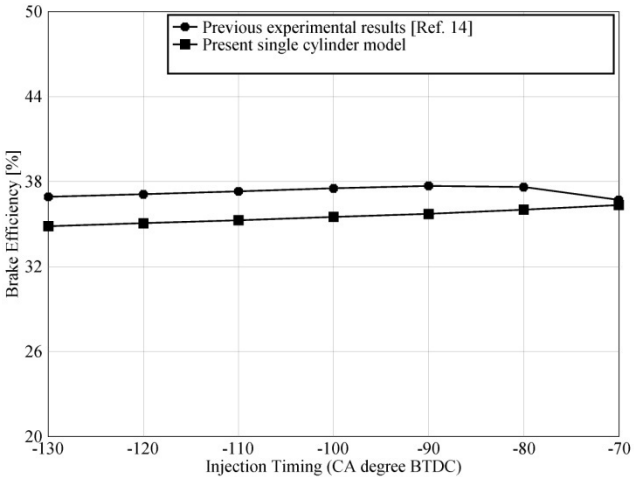

Fig. 6. Comparison between published experimental results.

Mohammadi *et al*. (2007) and present single cylinder direct injection engine model based on brake efficiency.

Engine Speed Influence on Injection Timing

In the present model, hydrogen was injected into the cylinder within a timing range started just before IVC (-96^0 BTDC) until TDC (0^0). AFR was varied. Amount of hydrogen injected in one cycle is approximately 22 mg/cycle with injection pulse duration of 4.4 ms. Engine speed was varied from 2000 rpm to 6000 rpm. Stoichiometric condition was fixed throughout the investigation.

Figure 7 shows the variation of indicated thermal efficiency with the injection timing for the changes of engine speed. It can be seen that the indicated efficiency increases with decreases of engine speed. From the acquired results, indicated efficiency increases slightly with advances of injection timing towards TDC for all

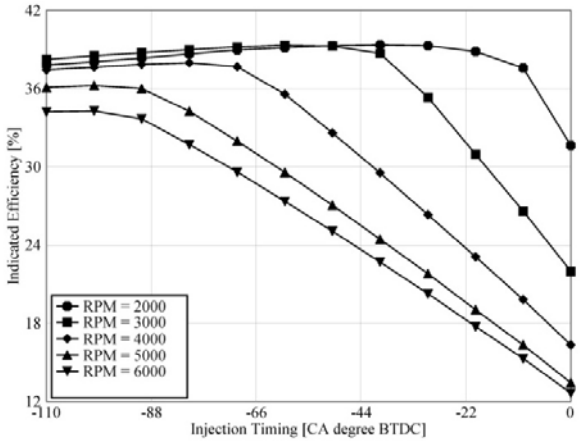

Fig. 7. Variation of indicated efficiency with injection timing for various engine speeds.

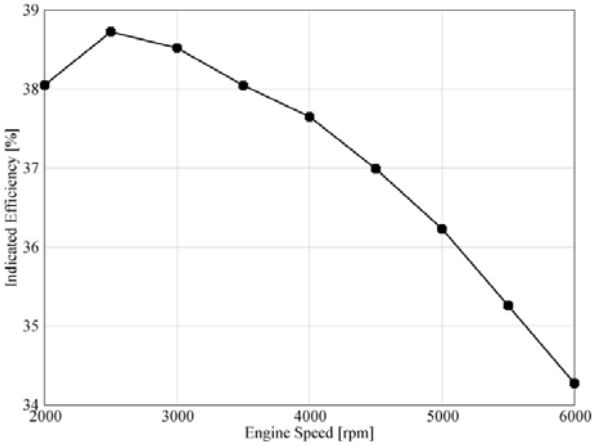

Fig. 8. Effect of engine speed on indicated efficiency.

engine speed range. It is also seen that the slightly increase of indicated efficiency until about 30^0 BTDC for 2000 rpm then it drops down. The rate of change in indicated efficiency is higher for higher speed and drop occurs early in higher speeds. For very high speeds, the drop happens earlier due to the early interaction between the injection duration and ignition timing. Optimum injection timing under speeds from 2000 rpm to 5000 rpm was in the range (40^0-80^0) BTDC while the optimum injection timing for 6000 rpm was 100^0 BTDC. Obviously, engine speed has a strong contribution in specifying the optimum injection timing. The very limited acceptable injection timing range occurs for high speeds. The selection of the proper injection timing is crucial not only for performance aspects, but also for stable operation. However, one should keep in mind that this situation, described currently, is for stoichiometric condition. It was extensively emphasized by related studies that stable stoichiometric operation is not simple in hydrogen engines and it is accompanied by lot of difficulties. So, with higher AFR best situation is expected. The variation of engine speed on the indicated efficiency is shown in figure 8 for stoichiometric operation and injection timing of 100^0 BTDC. It can be seen that the maximum indicated efficiency is 38.55% corresponding to engine speed 2500 rpm. This variation of indicated efficiency is primarily due to the variation of the volumetric efficiency.

Figure 9 shows the influence of injection timing on ISFC for different engine speeds. Lower engine speeds operation consumes smaller amounts of hydrogen as well as permits wider range for injection timing. The inverse is true for higher speeds where very limited range is available for injection timing. For 2000 rpm, the fuel consumption rates are acceptable throughout the studied range with injection timing of 60^0 BTDC being the optimum. At injection timing of 100^0 BTDC, minimum hydrogen consumed at 6000 rpm.

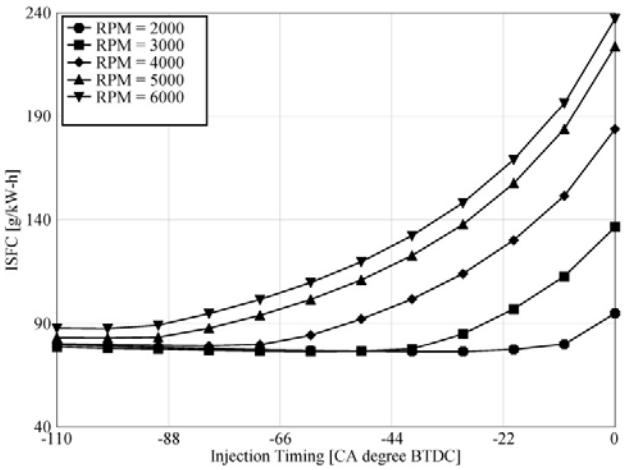

Fig. 9. Variation of ISFC with injection timing for various engine speeds.

Figure 10 illustrates the variation of power with injection timing with respect to changes the engine speed. It can be seen that the power gained increases with increases of engine speed except 6000 rpm case. However, this happens due to the interaction between injection duration and ignition timing. So, it does not represent the normal situation. This occurs at injection timing in the vicinity of TDC. The maximum power of 123 kW was gained at injection timing of 100^0 BTDC for 5000 rpm, while the optimum injection timing that gives at 2000 rpm was 40^0 BTDC and maximum power of 59 kW. The power shows a maximum at engine speed 5000 rpm. It is also observed that the power gained decreases at 6000 rpm due to the increase in the friction losses. The variation of engine speed on the power gained is shown in Fig. 11 for stoichiometric operation and injection timing of 100^0 BTDC. From the acquired results, the power increases slightly with advances of injection timing towards TDC for all engine speed range. It is also seen

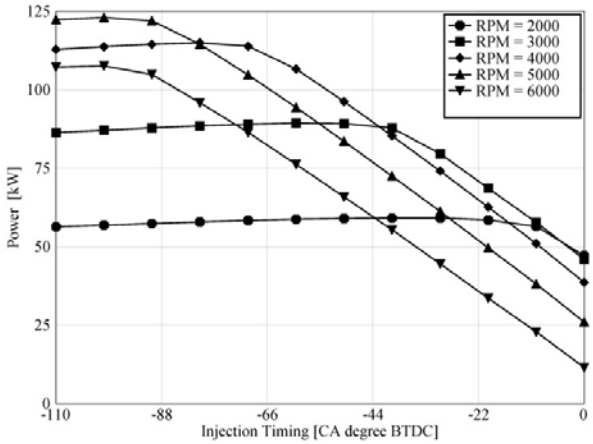

Fig. 10. Variation of power output with injection timing for various engine speeds.

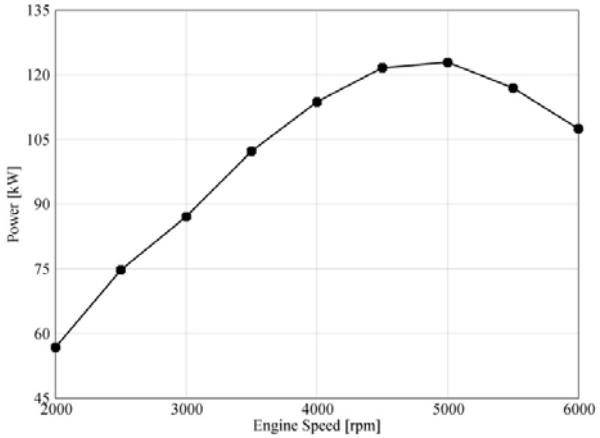

Fig. 11. Effect of engine speed on power.

that the slightly increase of power until about 30^0 BTDC for 2000 rpm then it drops down. The rate of change in power is higher for higher speed and drop occurs early in higher speeds. For very high speeds, the drop happens earlier due to the early interaction between the injection duration and ignition timing and friction losses.

Figure 12 shows the trends of torque with injection timing with the interaction of engine speed effect. Higher torques is produced at lower speed with extra advantages of more acceptable operation range of injection timing. The severe drop with high speed introduces a challenge for injection timing optimization. Based on torque measure, the optimum injection timing throughout the studied speeds, ranged from 40^0 BTDC at 2000 rpm until 100^0 BTDC at 6000 rpm. This extended range imposes more control difficulties. However, compromise solutions can be applied.

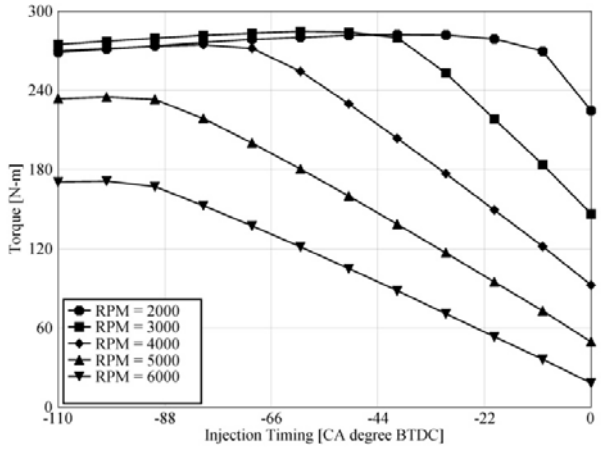

Fig. 12. Variation of torque output with injection timing for various engine speeds.

As a whole, there is optimum injection timing that gives the maximum efficiency, maximum power and torque and minimum desired indicated specific fuel consumption. This optimum injection timing strongly depends on the engine speed. Shorter injection duration is required at lean conditions compared to rich conditions. Long injection duration can interact with spark timing which is highly undesirable because of it causes the unstable operation. Therefore, short injection duration is reflected in more extended acceptable injection range. Although, spark timing is restricted with injection timing, the stable operation can be obtained in wide range of engine speed as long as spark timing is adequately selected.

CONCLUSIONS

A computational model was developed for four cylinders direct injection hydrogen fueled internal combustion engine. The main task was to find the optimum injection timing and investigate the influence of AFR and engine speed on this optimum value. The main results are summarized as follows:

1. The engine performance is strongly depends on the engine speed. The engine speed 2500 rpm gives the maximum indicated efficiency.
2. Optimum injection timing depends also strongly on engine speed. Lower speeds advances optimum injection timing toward TDC timing.
3. As a compromise, injection timing of 60^0 BTDC can be considered as optimum for the present engine. However, this is for constant injection timing. The recommended operation is with different injection timing bases on engine speed.
4. Interaction between injection duration and spark timing is strongly undesired and can result in unstable operation. This is was apparent by the unaccepted performance parameters during interaction period. Avoidance of this interaction should take priority in specifying injection timing.
5. Spark timing is another parameter that should be optimized for hydrogen engines, especially direct injection hydrogen engines. The optimum values of

spark timing and injection timing are related strongly. The best way of optimizing injection timing is to fix spark timing on maximum brake torque timing.

ACKNOWLEDGMENTS

The authors would like to express their deep gratitude to Universiti Malaysia Pahang (UMP) for provided the laboratory facilities and financial support.

REFERENCES

Eichlseder, H., Wallner, T., Freymann, R. and Ringler, J. 2003. The potential of hydrogen internal combustion engines in a future mobility scenario. SAE 2003- 01-2267.

Kahraman, E., Ozcanlı, C. and Ozerdem, B. 2007. An experimental study on performance and emission characteristics of a hydrogen fuelled spark ignition engine. Int J Hydrogen Energy 2007. 32:2066-2072.

Kim, JM., Kim, YT., Lee, SY. and Lee, JT. 1995. Performance characteristics of hydrogen fueled engine with the direct injection and spark ignition system. SAE paper no. 952498.

Kim, YY., Lee, JT. and Caton, JA. 2006. The development of a dual-Injection hydrogen-fueled engine with high power and high efficiency. Journal of Engineering for Gas Turbines and Power, ASME. 128:203-212.

Kim, YY., Lee, JT. and Choi, GH. 2005. An investigation on the cause of cycle variation in direct injection hydrogen fueled engines. Int. J. Hydrogen Energy. 30:69-76.

Lee, JT., Kim, YY. and Caton, JA. 2002. The development of a dual injection hydrogen fueled engine with high power and high efficiency. Proceedings of the 2002 fall technical conference of the ASEM internal combustion engine division. 323-33.

Lee, JT., Kim, YY., Lee, CW. and Caton, JA. 2001. An investigation of a cause of backfire and its control due to crevice volumes in a hydrogen fueled engine. Trans ASME. 123:204-10.

MacCarley, CA. and Van Vorst, WD. 1980. Electronic fuel injection techniques for hydrogen energy. Int J Hydrogen Energy. 5:179-203.

Mohammadi, A., Shioji, M., Nakai, Y, Ishikura, W. and Tabo, E. 2007. Performance and combustion characteristics of a direct injection SI hydrogen engine. Int J Hydrogen Energy. 32:296-304.

Nakagawa, Y., Nakai, M. and Hamai, K. 1982. A study of the relationship between cycle-to-cycle variations of combustion and heat release delay in a spark-ignited engine. JSME. 25:54-60.

Rottengruber, H., Berckmüller, M., Elsässer, G., Brehm, N. and Schwarz, C. 2004. Direct-injection hydrogen SI-engine operation strategy and power density potentials. SAE paper No. 2004-01-2927.

Sierens, R., Verhelst, S. and Verstraeten, S. 2005. An overview of hydrogen fuelled internal combustion engines. Proceedings International Hydrogen Energy Congress and Exhibition IHEC 2005 Istanbul, Turkey. pp. 1-12.

Stockhausen, WF., Natkin, RJ., Kabat, DM., Reams, L., Tang, X., Hashemi, S, Szwabowski., SJ. and Zanardelli, VP. 2002. Ford P2000 Hydrogen Engine Design and Vehicle Development Program. SAE Paper No.2002-01-0240.

Tang, X., Kabat, DM., Natkin, RJ., Stockhausen, WF. and Heffel, J. 2002. Ford P2000 Hydrogen Engine Dynamometer Development. SAE Paper No.2002- 01-0242.

Tsujimura, T., Mikami, A. and Achiha, N. 2003. A Study of Direct Injection Diesel Engine Fueled with Hydrogen. SAE paper No. 2003-01-0761.

Varde, KS. and Frame, GA. 1985. Development of a high-pressure hydrogen injection for SI engine and results of engine behavior. Int. J. Hydrogen Energy. 10(11):743-48.

White, CM, Steeper, RR. and Lutz, AE. 2006. The hydrogen-fueled internal combustion engine: a technical review. Int. J. Hydrogen Energy. 31:1292–1305.

Stockhausen, WF., Natkin, RJ., Kabat, DM., Reams, L., Tang, X., Hashemi, S., Szwabowski, SJ. and Zanardelli, V. 2002. Ford P2000 hydrogen engine design and vehicle development program. SAE 2002- 01-0240.